Proc. Lunar Planet. Sci. Conf. 11th (1980), p. 2075–2097.
Printed in the United States of America

Impact cratering in viscous targets: Laboratory experiments

R. Greeley[1]*, J. Fink[1], D. E. Gault[2], D. B. Snyder[1], J. E. Guest[3], and P. H. Schultz[4]

[1]Center for Meteorite Studies and Department of Geology, Arizona State University, Tempe, Arizona 85281; [2]Murphys Center for Planetology, Murphys, California 95247; [3]University of London Observatory, Mill Hill Park, London NW7 2QS, England; [4]Lunar and Planetary Institute, Houston, Texas 77058

Abstract—Martian multilobed craters ("splosh" craters, rampart craters, etc.) may involve fluidization of ejecta as a result of entrained water, melted/vaporized ice, and/or aerodynamically decelerated ejecta. To determine the effects of target viscosity and yield strength on the formation and morphology of impact craters, 75 experiments were carried out in which target properties and impact energies were varied. The following sequence was observed in high speed motion pictures of the experiments: 1) initial impact of projectile; 2) excavation of crater and rise of ejecta plume; 3) formation of a transient central mound which collapses generating a surge of material which can partly override the plume deposit; 4) oscillation of the central mound (in high energy impacts and fluid targets) with progressively smaller surges of material leaving the crater. The oscillating mound may "freeze" as either a peak or a depression. Dimensional analysis of the experimental results indicates: 1) dimensions of the central mound are proportional to the energy of the impacting projectile, and to the inverse of both the yield strength and viscosity of the target material; 2) for most of the impact experiments, effects of target viscosity appear to have been relatively minor and the target muds behaved essentially as inviscid fluids; the cratering process thus represented a balance between projectile kinetic energy and the potential energy required to excavate the initial transient cavity (i.e., gravity scaling); 3) extrapolation of these experimental results to large martian craters requires that the effective viscosity of the surface layer(s) must be less than 10^{10} poise, which is compatible with estimates for terrestrial debris flows. Multilayer targets influence the ejecta morphology: a thin "dry" layer (i.e., "regolith" or icy crust) on top of the viscous mixture retarded the emplacement of ejecta, whereas a thin fluid (water) layer on top of the mixture lubricated the ejecta and enhanced flow. These results may be applicable to interpretation of martian craters and to impacts into outer planet satellites composed of ice-silicate mixtures such as Callisto and Ganymede.

1.0 INTRODUCTION

One of the more striking discoveries of the Viking mission is the presence of unusual forms of impact crater ejecta, facies, or deposits. Although differences between lunar and martian craters were first indicated by Mariner 9 images, the high quality Viking Orbiter images revealed an unexpectedly wide range of ejecta

* also Space Sciences Division, NASA Ames Research Center, Moffett Field, California 94035

morphologies, from typical lunar and mercurian forms to types suggestive of ejecta emplacement as a fluidized mass (Carr *et al.*, 1977). These crater forms, variously termed "splosh" craters, ejecta-flow craters, and rampart craters, all termed *multilobed craters* herein, do not occur on the "dry" atmosphere-free planets Mercury and Moon, and it has been suggested that water and/or the atmosphere of Mars may somehow be responsible for the flow-like nature of the ejecta. Several photogeologic studies of martian craters have attempted to determine geometric crater relationships (diameter versus ejecta lobe size, etc.) and establish their occurrence as functions of parameters such as latitude, elevation, terrain type and geologic age (Mouginis-Mark, 1979; Mutch and Woronow, 1980; Johansen, 1978; and others). In addition to the photogeologic studies, some investigators have studied the effects of the thin martian atmosphere on ejecta emplacement (Schultz and Gault, 1979) and considered possible terrestrial analogs (Roddy *et al.*, 1979).

Our approach to the problem has been two-fold: 1) laboratory experiments using the NASA Ames Vertical Ballistic Gun Facility, and 2) photogeologic studies to provide a basis of comparison for the laboratory results. Exploratory experiments involving cratering in viscous clay have been reported previously (Gault and Greeley, 1978), as has consideration of viscous deformation of craters (Scott, 1967); results of our photogeologic studies will be reported later. Here we discuss impacts in clay targets under controlled conditions, and discuss the implications for the formation of multilobed ejecta deposits, central peaks and central pits. Not only may these experiments be applicable to impact craters on Mars and Earth, but they may have implications for cratering on the volatile-rich outer planet satellites and general cratering processes as well.

2.0 LABORATORY EXPERIMENTS

The primary objective of the experiments was to determine the effect that target rheological properties have on crater and crater ejecta morphology. The Ames Facility is ideally suited for such experiments because target and impact conditions can be controlled, and because high speed motion pictures obtained during impact permit assessment of the processes of crater formation and ejecta emplacement. The facility consists of a target chamber 2.5 m in diameter by 2.5 m high that can be evacuated to martian atmospheric pressures. In these experiments, chamber pressure ranged from about 15 to 50 mb. These pressures were utilized in order to prevent freezing of the water contained in the target material. Impact velocities ranged from 5×10^2 m s^{-1} to 5.5×10^3 m s^{-1}; impact projectiles included 3.175×10^{-3} m, 4.77×10^{-3} m, and 6.35×10^{-3} m glass, aluminum and steel spheres, giving a range of impact energies from 6.9 joules to 2.2×10^3 joules. The target material was contained in one of two cylindrical buckets (small = 0.60 m in diameter by .205 m deep; large = 0.91 m in diameter by 0.46 m deep) fitted in a flat floor 2.5 m in diameter; target material was placed in the bucket so that it formed a nearly continuous surface with the floor. Ideally, the target should be of very large or of infinite dimension, so as to reduce or eliminate boundary

effects. Such conditions cannot be achieved in the laboratory, and the target buckets used in these experiments are the same as in previous investigations (e.g., Gault and Wedekind, 1977) to allow comparisons with other target materials. Two types of target materials were used: potters clay mixed with either silicon oil or with water. Silicon oil was used as a fluid because it does not freeze and it is relatively stable to atmospheric pressures of about 15 mb. Clay/water targets were used for more complex models involving mud, and multilayered ice/viscous mud targets.

A series of 75 successful impacts was completed in which three parameters were varied: target viscosity, impact energy and angle of impacting projectile with respect to target (Table 1). The first series was divided into subsets A through J. In each subset, target viscosity was held nearly constant while impact energies and angles were varied. In the last shot of each subset, a 1 cm layer of dry clay was emplaced on the mud to produce a multilayered target. After the shot, the dry clay was mixed with the underlying mud to increase the viscosity for the next subset, and the procedure was repeated. The rheological properties (viscosity and yield strength) of the target material were measured for each subset of experiments, using a sample collected from the target bucket. For the homogeneous, non-layered, targets (#1–8, 11–14, 17–27, 31, and 33–36) the apparent viscosity was measured directly with a Brookfield viscometer Model HBT, *in situ,* both immediately before and after impact using a disk-type spindle of known surface area at a rotational speed of 10 RPM. Plastic viscosities and yield strengths were calculated for batches of slurry extracted every 2 to 7 runs, whereas apparent viscosities were measured during every run. The rheological behavior of the target materials is discussed in detail in Appendix I.

During impact, the cratering events were filmed with high speed motion pictures (400 frames s^{-1}). After each shot, color and black and white photographs were taken and various measurements were made of the crater and ejecta deposits. Subsequent analyses of the motion pictures enabled measurement of various transient features such as ejecta plume angle.

3.0 EXPERIMENTAL RESULTS

In this section we present a general model of crater formation and ejecta emplacement observed for impacts in viscous targets and discuss possible correlations.

3.1 General laboratory model

Analyses of high speed motion pictures lead to a general model of cratering in viscous media (Figs. 1,2). Following the terminology of Gault *et al.* (1968) for a three-stage cratering process, during the initial *compression stage* in which jetting occurs, there is no apparent difference between impacts in dry targets and viscous targets. During the *excavation stage,* however, a slight bulge on the surface of the target material is pushed ahead of the expanding ejecta plume; in

Table 1. Impact crater experiment data. Pre-impact data: target density (ρ = kg-m^{-3}), apparent viscosities at various rotation rates [η_A(RPM) = kg-m^{-1}-s^{1}], calculated plastic viscosities (η_p) and yield strengths (τ = kg-m^{-1}-s^{-2}); type of slurry fluid (oil = O; water = W); target configuration (R = uniform slurry; P = powder surface layer; W = water surface layer; S = sand surface layer; N = newspaper surface layer; I = ice surface layer; D = doublet: two shots into same target; T = two clay layers separated by dry powder or newspaper); projectile mass (m = kg), velocity (v = m-s^{-1}), angle of impact (A_s = degrees); chamber pressure at time of impact (P = mm Hg).

Post impact data: central peak height (h_m = m), apex angle (A_m) and basal diameter (D_m); ejecta plume angle (A_p) and plume deposit diameter (D_p); surge deposit diameter (D_s); and crater diameter (D_c). Not all data were obtainable for each run.

		Target properties							Impact conditions				Crater features							
Subset	Run #	ρ kg-m^{-3}	η_P kg-m^{-1}s^{-1}	η_A kg-m^{-1}s^{-1}	RPM	τ kg-m^{-1}s^{-2}	Clay base	Target config.	m $\times 10^{-5}$kg	v $\times 10^{3}$m-s^{-1}	A_s deg.	P mm Hg	h_m m	D_m m	A_m deg.	D_p m	A_p deg.	D_s m	D_c m	Shot number
Series I																				
A	1*	1540	2.26	10.6	10.0	4.74	O	R	4.56	0.55	90	19.0	0.107	0.178	58	0.44	73	—	—	790634
	2*	1540	2.26	10.6	10.0	4.74	O	R	37.35	1.80	90	19.5	0.425	—	58	—	75	1.34	—	790635
	3*	1550	2.26	10.4	10.0	4.74	O	R	37.35	1.84	90	18.0	0.383	0.672	64	—	77	1.29	—	790636
	4	1550	2.26	11.5	10.0	4.74	O	P	37.40	2.06	90	16.0	0.325	0.463	55	0.71	60	—	—	790701
B	5*	1560	2.77	13.8	10.0	7.72	O	R	4.60	1.15	90	30.0	0.132	0.229	70	0.46	73	—	—	790702
	6*	1560	2.77	14.7	10.0	7.72	O	R	37.23	1.57	90	15.0	0.355	0.621	55	1.45	74	1.25	—	790703
	7	1560	2.77	14.4	10.0	7.72	O	R	37.23	1.71	15	12.0	0.215	0.386	56	1.14	67	—	—	790704
	8	1560	2.77	15.5	10.0	7.72	O	R	37.36	1.36	15	20.0	0.241	0.471	52	1.32	68	1.00	—	790705
	9	1580	—	—	—	—	O	P	37.36	2.09	90	25.0	—	—	—	—	—	—	—	790706
	10	1580	—	—	—	—	O	P	161.50	1.49	90	16.0	0.696	0.401	—	—	58	0.55	—	790708
C	11*	1580	2.29	72.3	5.0	6.43	O	R	4.56	1.09	90	18.0	0.089	0.216	80	0.57	73	—	0.290	790709
	12*	1580	2.29	65.6	5.0	6.43	O	R	37.36	1.87	90	18.0	0.301	0.617	61	1.60	74	0.98	—	790710
	13*	1580	2.29	38.4	5.0	6.43	O	R	15.93	1.55	90	10.0	0.190	0.345	59	0.80	74	—	—	790711
	14*	1580	2.29	32.0	5.0	6.43	O	R	10.55	1.72	90	19.0	—	—	—	1.50	—	—	—	790713
	15	1580	2.29	—	—	6.43	O	R	29.97	2.06	15	15.0	0.181	0.305	68	0.50	68	—	—	790716
	16	1580	2.29	—	—	6.43	O	R	29.04	0.81	15	12.0	0.057	0.127	99	—	66	—	0.170	790719
	17	1580	2.14	36.8	10.0	4.60	O	P	37.29	3.78	90	9.0	0.200	0.397	66	0.57	47	—	—	790721
D	18*	1640	9.20	44.8	10.0	33.97	O	R	15.88	1.07	90	14.0	0.090	0.228	100	0.51	73	—	0.360	790722
	19*	1640	9.20	61.6	10.0	33.97	O	R	10.56	1.72	90	16.0	0.156	0.412	96	—	70	—	0.600	790723
	20	1640	9.20	—	—	33.97	O	R	30.00	2.03	15	7.0	0.051	0.156	110	—	67	—	0.290	790725
	21*	1640	9.20	48.0	10.0	33.97	O	R	15.90	5.24	90	4.5	0.248	0.436	79	0.80	67	—	0.560	790726
	22	1640	9.20	25.6	5.0	33.97	O	R	30.00	4.33	15	6.0	0.026	0.091	130	—	60	—	0.250	790728
	23	1640	9.20	96.0	5.0	33.97	O	W	37.27	2.19	90	4.0	0.278	0.366	58	0.630	70	—	—	790731
	24	1640	9.20	96.0	5.0	33.97	O	W	106.20	1.71	90	19.0	0.379	0.521	48	1.320	75	1.04	—	790732
	25	1640	9.20	155.0	5.0	33.97	O	P	37.36	5.35	90	10.0	0.304	0.385	67	—	43	—	—	790733

1980LPSC...11.2075G

E	26*	1720	10.87	160.0	10.0	39.81	O	R	15.82	1.62	90	21.0	—	—	—	0.570	71	—	0.343	790734
	27*	1720	10.87	176.0	10.0	39.81	O	R	37.29	1.57	90	19.0	0.050	0.237	131	0.708	76	—	0.520	790735
	28	1720	10.87	—	—	39.81	O	R	105.50	1.48	90	22.0	0.160	0.319	81	0.855	77	—	0.776	790736
	29	1720	10.87	—	5.0	39.81	O	R	29.90	1.95	15	21.0	—	—	—	1.850	66	—	0.315	790737
	30	—	—	—	—	—	O	P	106.30	1.51	90	28.0	—	—	—	—	—	—	—	790739
F	31	1760	—	122.0	10.0	—	O	R	15.94	1.54	90	20.0	—	—	—	—	—	—	—	790740
	32	1760	—	—	—	—	O	R	15.91	1.80	90	21.0	—	—	—	—	59	—	0.273	790741
	33	1760	—	275.0	5.0	—	O	R	37.65	1.79	90	20.0	—	—	—	—	—	—	—	790742
	34	1760	—	256.0	5.0	—	O	R	29.91	2.03	90	20.0	—	—	—	—	—	—	—	790744
	35	1760	—	243.0	5.0	—	O	D	37.62	2.11	90	20.0	—	—	—	—	62	—	0.456	790745
	36	1760	—	237.0	5.0	—	O	D	15.94	1.62	90	19.0	—	—	—	—	—	—	0.210	790746
	37	1760	—	—	—	—	O	R	12.59	1.47	15	20.0	—	—	—	—	65	—	0.143	790747
G	38	1800	13.75	256.0	5.0	0.11	W	R	4.69	1.01	90	30.0	—	—	—	—	64	—	0.266	790749
	39	1800	13.75	179.0	5.0	0.11	W	R	37.57	0.55	90	30.0	—	—	—	—	68	—	0.473	790750
	40	1800	13.75	198.0	5.0	0.11	W	W	12.52	1.02	90	100.0	—	—	—	—	68	1.23	0.325	790751
H	41	1770	1.93	57.6	5.0	6.92	W	R	4.67	1.64	90	30.0	—	—	—	—	65	—	0.227	790752
	42	1770	—	—	—	210.00	W	R	15.93	2.22	15	32.0	0.018	0.068	—	—	62	—	0.271	790754
	43	1770	—	115.0	2.5	210.00	W	R	37.59	2.07	90	31.0	0.050	0.275	120	—	63	—	0.511	790755
	44	1770	—	102.0	2.5	210.00	W	R	105.49	1.53	90	30.0	0.077	0.382	144	0.726	68	—	—	790756
	45	1770	—	141.0	2.5	210.00	W	R	37.29	2.29	90	26.0	—	—	—	0.717	70	—	0.900	790757
I	46	1730	1.56	54.4	5.0	12.42	W	T	15.96	0.92	15	26.0	—	—	—	—	68	—	0.224	790758
	47	1730	1.56	57.6	5.0	12.42	W	R	4.61	1.61	90	27.0	—	—	—	—	69	—	0.269	790759
	48	1730	1.56	70.4	5.0	12.42	W	R	15.68	1.85	90	26.0	0.032	0.200	150	—	70	—	0.466	790760
	49	1730	1.52	60.8	5.0	12.42	W	R	37.28	1.92	90	14.0	0.054	0.343	144	—	69	—	0.583	790762
	50	1730	1.52	80.0	5.0	12.42	W	R	4.67	5.49	90	10.0	—	—	—	—	68	—	0.432	790763
J	51	1800 1730	—	173.0 80.0	5.0	—	W W	T	37.28	2.17	90	16.0	—	—	—	0.470	65	—	0.191	790764
	52	? 1760	—	102.0 141.0	5.0	—	W	T	37.26	2.05	90	12.0	—	—	—	—	69	—	0.469	790765
	53	1550	1.61	39.2	10.0	22.96	W	R	3.69	1.03	90	50.0	0.081	0.191	93	0.313	72	—	—	790766
	54	1550	1.61	45.6	10.0	22.96	W	R	3.78	2.12	90	40.0	0.120	0.236	85	0.448	75	—	0.236	790767
	55	1620 1550	—	150.0 45.6	5.0 10.0	—	W W	T	37.29	2.17	90	16.0	0.216	0.417	63	0.681	68	—	0.477	790768

Table 1. *(Continued)*

Subset	Run #	Target properties: ρ kg-m^{-3}	η_P kg-m^{-1}s^{-1}	η_A kg-m^{-1}s^{-1}	RPM	τ kg-m^{-1}s^{-2}	Clay base	Target config.	Impact conditions: m $\times10^{-5}$kg	v $\times10^{3}$m-s^{-1}	A_s deg.	P mm Hg	Crater features: h_m m	D_m m	A_m deg.	D_p m	A_p deg.	D_s m	D_c m	Shot number
Series II																				
	56	1604	—	84.0 110.0	10.0	—	O W	T	37.63	1.40	90	120.0	—	—	—	0.762	—	—	0.585	791207
	57	1604	—	—	—	—	O W	T	4.59	1.56	90	110.0	—	—	—	—	—	—	0.356	791208
	58	1614	—	—	—	—	W	R	4.59	1.50	90	60.0	—	—	—	—	—	—	0.380	791209
	59	1614	—	—	—	—	W	N	4.63	1.60	90	120.0	—	—	—	—	—	—	0.330	791210
	60	1614	—	230.0 —	10.0 —	—	O W	T	37.66	2.06	90	54.0	—	—	—	—	—	—	0.380	791211
	61	1747 1611	—	310.0 —	10.0 —	—	W W	T	37.66	2.00	90	90.0	—	—	—	—	—	—	0.410	791212
	62	1761 1699	—	880.0 —	10.0 —	—	W W	T	37.66	2.20	90	120.0	—	—	—	0.430	—	—	0.290	791213
	63	1761 1666	—	760.0 —	10.0 —	—	W W	T	37.68	2.18	90	80.0	—	—	—	0.650	—	—	0.540	791214
	64	1755 1690	—	1040.0 280.0	10.0	—	W W	T	37.61	2.06	90	40.0	—	—	—	—	—	—	0.380	791216
	65	1840 1740	—	1400.0 445.0	10.0	—	W W	T	37.64	2.13	90	80.0	—	—	—	0.470	—	—	0.305	791217
	66	1745 2020	—	480.0 1150.0	10.0	—	W W	T	37.60	2.07	90	—	—	—	—	—	—	—	0.219	791218
	67	1720	—	620.0	10.0	—	W	R	4.43	1.90	90	40.0	—	—	—	—	—	—	0.203	791219
	68	1770 1720	—	560.0 620.0	10.0	—	W	I	37.65	2.20	90	2.00	—	—	—	—	—	—	0.140	791220
	69	1670	—	570.0	10.0	—	W	I	37.71	2.21	90	6.00	—	—	—	0.380	—	—	0.330	791221
	70	1610	—	225.0	10.0	—	W	I	4.72	2.09	90	10.00	—	—	—	—	—	—	0.210	791222
	71	1638	—	220.0	10.0	—	W	I	4.45	1.70	90	45.00	—	—	—	—	—	—	0.241	791224
	72	1638	—	240.0	10.0	—	W	I	4.45	1.80	90	25.00	—	—	—	—	—	—	0.162	791225
	73	1638	—	240.0	10.0	—	W	I	37.69	2.18	90	6.00	—	—	—	—	—	—	0.318	791226
	74	1620	—	280.0	10.0	—	W	R	4.41	2.10	90	10.00	—	—	—	0.430	—	—	0.203	791227
	75	1610	—	155.0	10.0	—	W	S	4.56	2.01	90	80.00	—	—	—	0.254	—	—	0.203	791228

* denotes shots used in Figs. 5–7.

some cases, this bulge is preserved as a remnant of the initial crater rim. The angle the expanding ejecta plume makes with the target surface appears to be inversely proportional to target strength or cohesion. Thus, the plume angle is quite steep in water, decreases with thicker clay slurries, and is lowest in dry sand (Fig. 3). The initial ejecta plume appears to be composed of discrete parcels of ejecta which quickly merge to form a relatively continuous sheet (Fig. 2). The expanding plume then tears into discrete segments when tensional stresses exceed material cohesion. This, too, appears to be qualitatively related to viscosity, ranging from a nearly continuous ejecta plume for water, to large "plates" or clots for very fluid clay, to small pieces for more viscous clay, and finally to individual grains for dry sand targets. The effect on ejecta morphology is shown in Fig. 4, in which the more fluid targets display well defined continuous outer boundaries progressing to the more familiar lunar-type "dry" ejects deposits consisting of various facies (continuous ejecta, discontinuous ejecta, bright rays).

The greatest and perhaps most significant differences between impacts in dry and viscous targets occur during the *post-impact modification* stage (Fig. 2). When the transient cavity reaches its maximum depth, isostatic adjustment begins immediately; the rapidity and magnitude of the adjustment being greater with decreasing viscosity. In relatively fluid targets, the recovery of the floor is so rapid that a rebounding central mound develops, its maximum height varying directly with impact energy and inversely with target viscosity and strength. Gravitational collapse of the central mound generates a surge of material that in some cases is sufficient to surmount the crater rim, sending a blanket of material over earlier emplaced ejecta plume deposits, although the radial extent of this surge is less than that of the plume deposit. The extent of the surge deposit is a function of central mound height, crater rim height, and fluidity of the target material.

Depending upon impact energy and target viscosity, the central mound may oscillate, forming a series of central mounds of decaying heights. Each of these mounds may produce a surge deposit of lesser and lesser extent, with the later units not having sufficient energy to surmount the crater rim. Oscillation was greatest in the very fluid targets, and in most cases the crater rim was not preserved as a topographic form after oscillation ceased. Oscillation of the central mound ceases when the energetic forces from the impact are dissipated and shear stresses are less than the yield strength of the target. The mound may "freeze" in a negative position (forming a central depression), depending also on the target strength.

Immediately after some shots, the target material in and near the impact zone actively degassed; evidently the impact released volatiles from the clay-water and clay-oil mixtures, fluidizing the target material. The effect was two-fold: in 74 percent of the impacts there was a decrease in target viscosity after impact (measured *in situ* before and after impact), and the post-impact fluidized material smoothed out irregularities in the floors of some craters, giving them a flooded appearance.

Thus, in this general model for impacts into viscous targets at laboratory scales

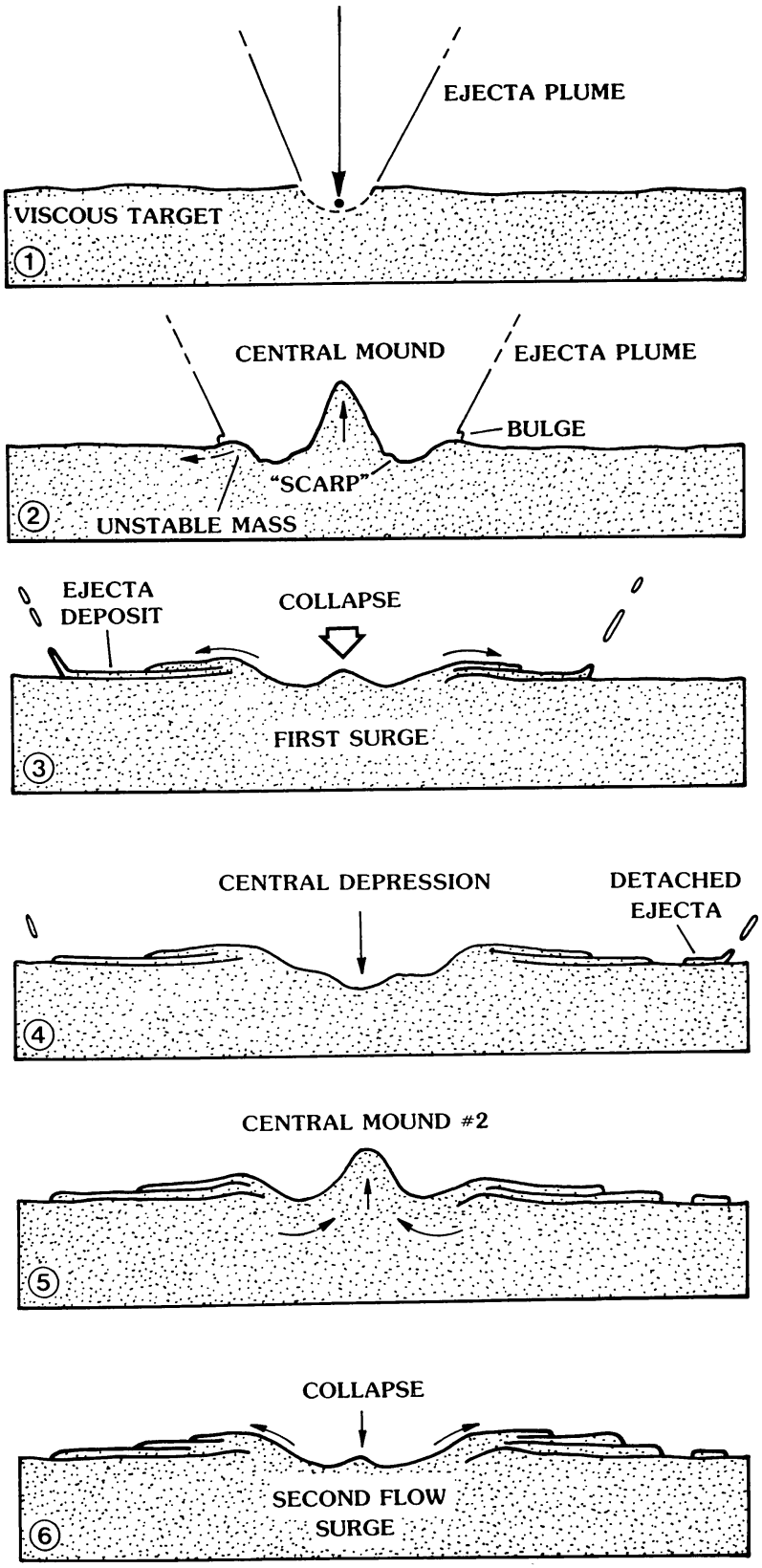

it is possible to produce multiple tiers of ejecta deposits, central peaks, flat floors, and central pits, all as functions of impact energies and target viscosity and strength. We point out, however, that after the generation of the first central mound in the experiments, subsequent oscillations may have been influenced by reflected waves from the walls and floor of the target bucket.

Impact at angles as low as 15° above the surface had no apparent effect on either the ejecta pattern or the crater morphology. In some experiments involving both normal and oblique impact angles, the collapsing central mound was asymmetric (perhaps because of slight inhomogenieties in the target) which resulted in asymmetric ejecta flow deposits.

The oscillation of the central mound may well be influenced by boundary effects of the target bucket, particularly in the high energy rounds. To determine these effects we recently ran a series of experiments ranging from very low energy shots in which the size of the crater was less than 1/20 of the bucket diameter, to high energy shots which clearly showed influence of the bucket walls. In all cases, oscillating central mounds could be produced if the ratio of impact energy to viscosity was high enough. (These results will be presented in more detail in a later paper.)

3.2 Dimensional analyses and functional relationships

In order to provide a basis for scaling to full size impacts, parametric relationships were sought in dimensionless form. Because our early experiments aimed to determine qualitative relationships, we varied many parameters and used slightly different recording techniques during different subsets of experiments. Of the total of 75 shots, 14 share sufficient conditions to be directly comparable. In the following discussion we consider only those experiments involving vertical impacts into homogeneous clay-oil targets. No multilayer targets are included.

Impact experiments into water (Gault and Wedekind, 1978), dry sand and soils, and rock (Gault, 1973; Gault and Wedekind, 1977) show that crater dimensions depend on impact energy, gravitational acceleration, and target strength. Crater diameter, for example, scales with the ¼ power of the impact energy for inviscid targets such as water and approximately with the ⅓ power of energy for targets

---

Fig. 1. Sequence of impact cratering in viscous targets derived from analysis of high speed motion pictures (compare to Fig. 2): 1) formation of ejecta plume; 2) rebound of floor produces a central mound; ejecta plume expands outward, pushing a small "bulge" of target material across the surface; ejecta plume begins to tear into discrete segments; 3) ejecta plume forms a deposit on the surface; gravitational collapse of central mound sends a surge of material up and over the transient crater rim to form a deposit overlying the ejecta plume deposits; 4) central mound oscillates to form a central depression, which in some cases "freezes" to leave a central pit; late-stage ejecta plume consists of discrete segments deposited as detached ejecta lobes; 5,6) oscillating central mound sends successive lobes of material over the rim to form terraced, superposed ejecta deposits. (Numbers refer to sequence, not time).

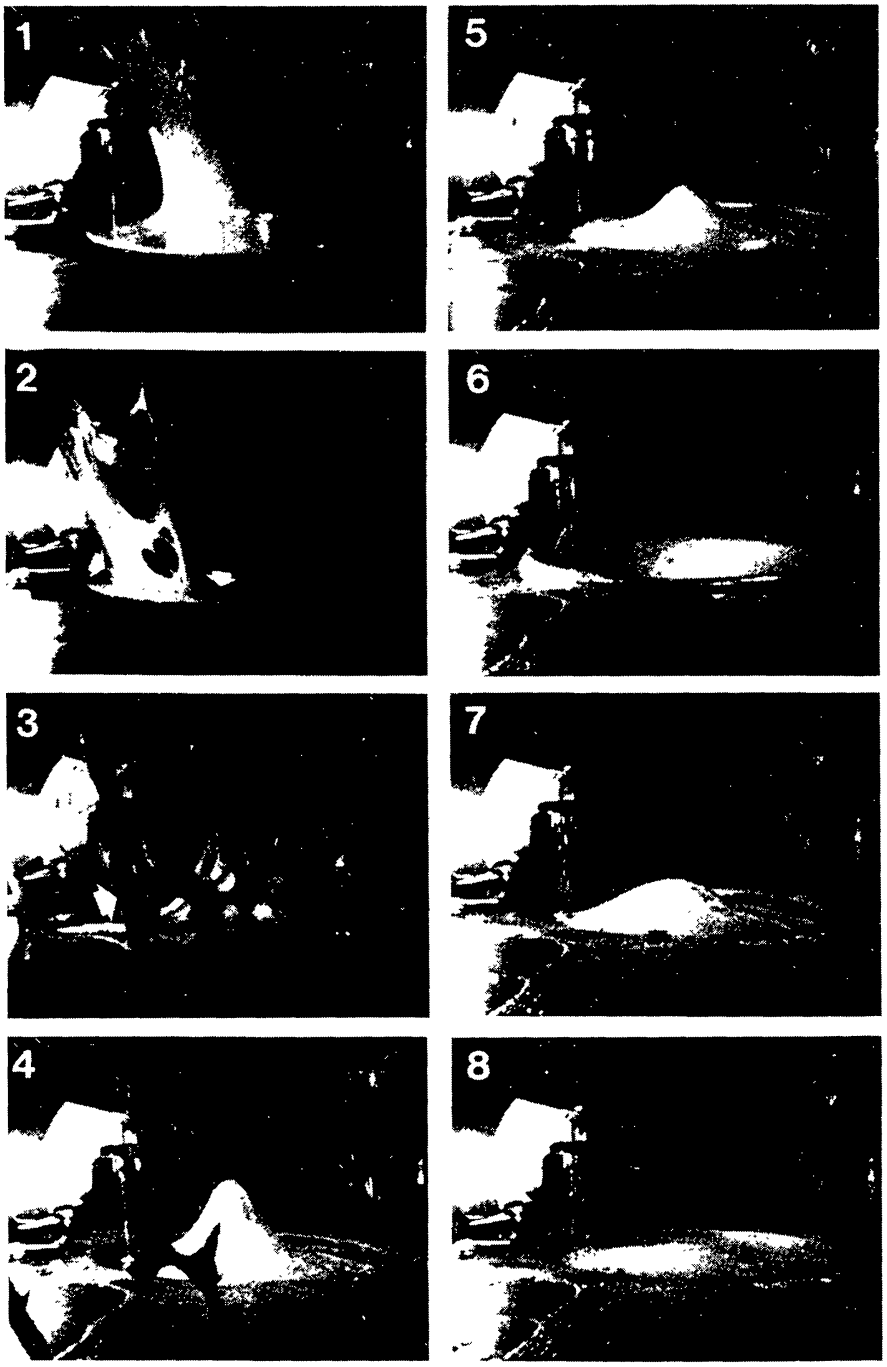

Fig. 2. Sequential frames from shot #6 (790703) showing impact in target having apparent viscosity of 150 poises (15 kg-m^{-1}-s^{-1}): 1) ejecta plume; 2) white arrows identify "bulge" of material being pushed ahead of expanding ejecta plume; ejecta plume begins to tear; 3) rising central mound is visible through "windows" in the expanding ejecta plume; 4) outline of target bucket visible; 5) central mound collapses, sending a surge of material (arrow in Frame 6) out of the bucket to be superimposed on the ejecta plume deposit (arrow in Frame 7); 8) due to low strength of target material, no crater topography was preserved. Device on the left of each frame is the viscometer.

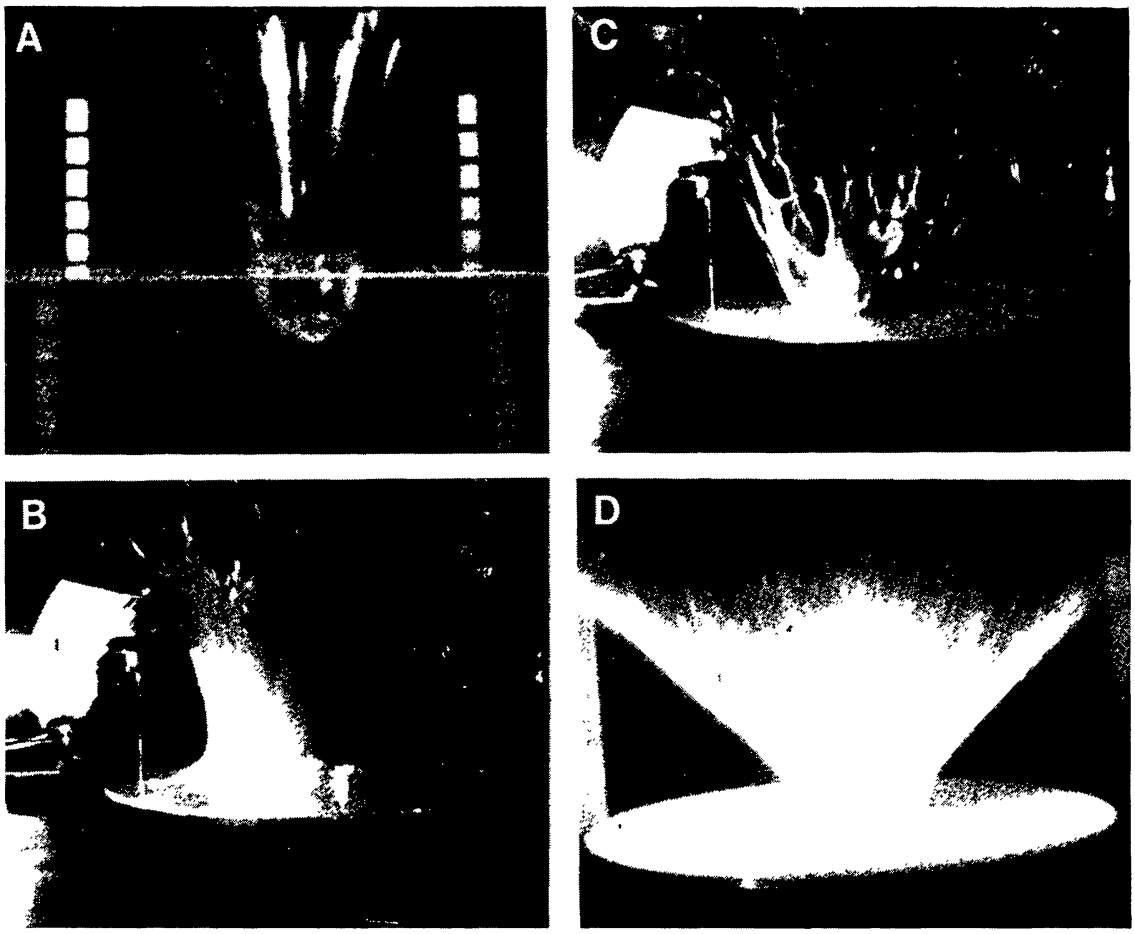

Fig. 3. Comparison of ejecta plume angles (A_p) for impacts in different target materials showing that increase in viscosity (η) leads to decrease in plume angle. A) Water ($\eta \sim 10^{-2}$P; $A_p = 75°$); B) "wet" clay slurry ($\eta \sim 10^{2}$P; $A_p = 70°$); C) stiff clay slurry ($\eta \sim 10^{3}$P; $A_p = 66°$); D) dry sand ($A_p = 58°$).

with high strength such as solid granite or basalt (Gault, 1973). Our current experiments employ target materials which are viscous and have a finite yield strength. Earlier exploratory impacts into viscous targets indicated that crater dimensions were proportional to the impact energy and to the inverse of the target viscosity (Gault and Greeley, 1978). To determine the relative influences of impact energy, target viscosity and yield strength on crater dimensions, we used dimensional analyses and combined the experimental variables into dimensionless groups. We considered six variables to be most important in the cratering process: impact energy (E); target viscosity (η), yield strength (τ), and density (ρ); gravitational acceleration (g); and some crater dimension (l) such as height of the central mound (h_m), average diameter of the ejecta plume deposit (D_p) or diameter of the final crater (D_c).

Of the many possible dimensionless groups, we first considered one which relates a crater dimension such as h_m to the energy of impact and the target weight

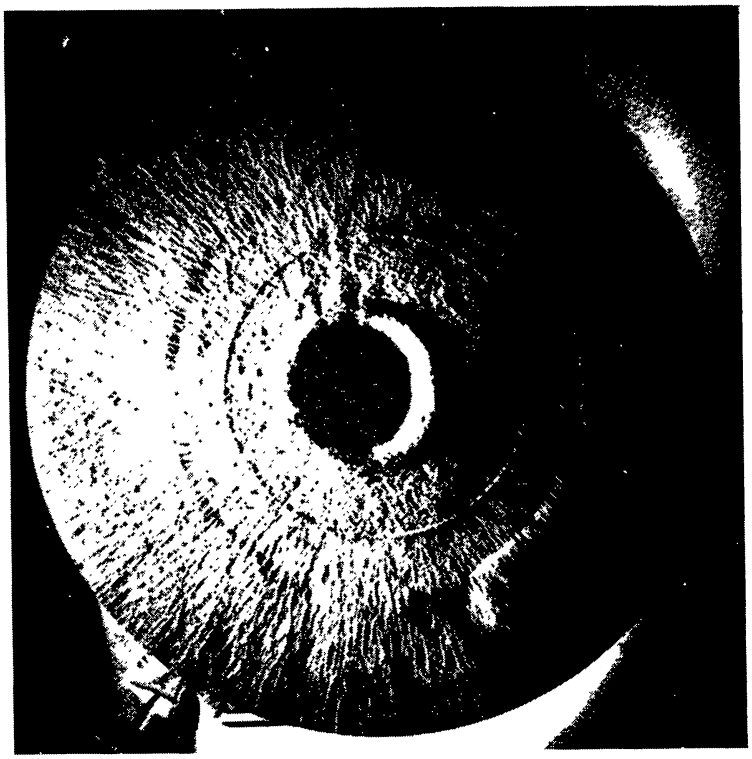

(a)

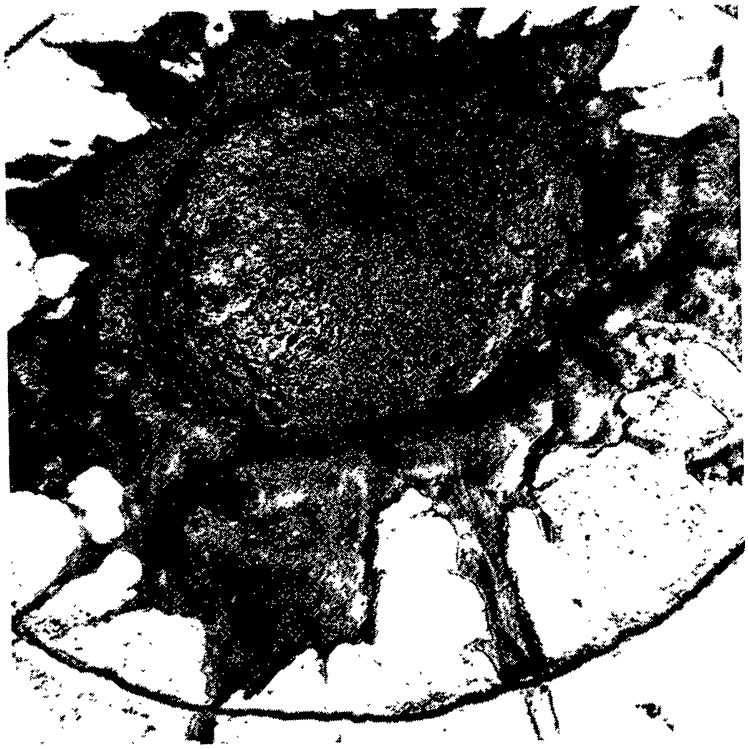

(b)

Fig. 4. Comparison of ejecta morphology for "dry" sand target (a) showing ragged "lunar" type deposits with that of an impact in viscous target (b) showing well defined ejecta boundary. (a) involved impact of pyrex sphere into dry pumice powder, (b) involved impact into clay-oil mixture.

(ρg). The group $\frac{E}{\rho g h_m^4}$ implies that the fourth power of the peak height should be proportional to the energy and the inverse of target weight. Thus, where this "gravity scaling" applies, large increases in impact energy, decreases in target density or decreases in gravitational acceleration all lead to relatively small increases in central peak height. This prediction was experimentally corroborated for the transient crater diameter by impacts into water (Gault and Wedekind, 1978).

A second scaling factor includes the influence of target strength, $\frac{E}{\tau h_m^3}$, which implies that for strength-dominated impacts, crater dimensions should scale as the ⅓ power of the energy divided by strength. This functional relationship was observed experimentally for impacts into targets of solid basalt and granite (Gault, 1973).

A third dimensionless group relates energy to viscosity, $\frac{\rho E}{\eta^2 h_m}$, and indicates that crater dimensions scale as the inverse of the square of viscosity. This second power dependence suggests that when viscosity effects operate, they have stronger influence on crater morphology than energy, gravity, target strength or density.

In our experiments we sought to determine the conditions under which gravity, target viscosity, or strength would dominate. We can determine the relative influences of yield strength and viscosity by comparing a viscous stress, $\eta^2/\rho h_m^2$, to yield strength, τ. For a typical experiment (all units m-k-s), $\tau \simeq 10$, $\eta \simeq 20$, $\rho \simeq 1500$, and $h_m \simeq 0.2$ (Table 1), so that $\eta^2/\rho h_m^2 = \frac{400}{(1500)(0.04)} \simeq 6 \simeq \tau$. Thus, strength and viscous effects should be comparable. Now considering gravitational stress, $\rho g h_m$, for the same conditions where $g \simeq 10$, we find $\rho g h_m \simeq 3000 \gg \tau \simeq \eta^2/\rho h_m^2$. Gravity effects should thus predominate in our experiments so that central mound height should scale as the ¼ power of the impact energy. The one exception is run #790735 (Figs. 5–7), where the calculated viscous stress was much larger than the gravity stress, due to the high target viscosity and low height of the central mound. In any such cases where strength or viscous effects apply, peak height should scale as a greater power of the impact energy, closer to ⅓ or 1.

In Figs. 5–7 we have plotted central peak height vs. different energy terms $E/\rho g$, E/τ and $\rho E/\eta^2$. Power law curves of the form $h = k(E^*)^n$, where E^* is the energy term and k and n are constants, were then fitted to the data. Figure 5 compares the effects of gravity and impact energy on mound height:

$$h_m = 0.7\left(\frac{E}{\rho g}\right)^{0.28}, \text{ r (correlation coefficient)} = 0.82.$$

Mound height exhibits only a slightly greater dependence on energy (0.28 vs. 0.25) than the fourth root scaling expected if gravity alone were modifying the

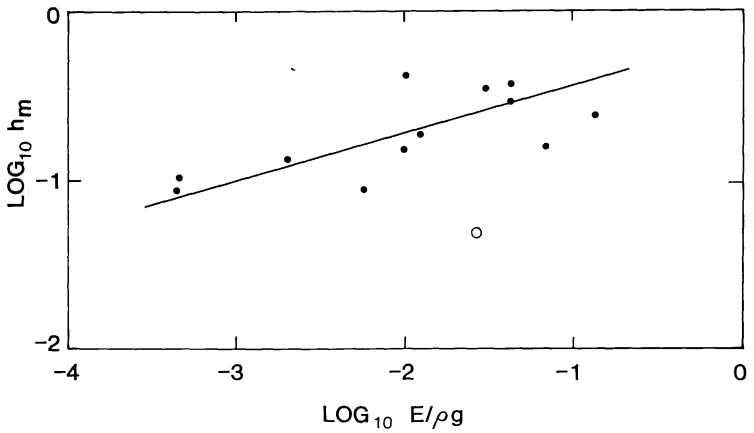

Fig. 5. Plot of maximum central mound height (h_m) as a function of gravity (g), target density (ρ) and energy (E); correlation coefficient = 0.82. Open circle = shot #790735 (see text).

crater morphology, and this difference is probably not statistically significant here.

Figure 6 shows the effect of the yield strength and indicates a closer correlation with the theoretically predicted ⅓ root scaling for mound height:

$$h_m = 0.8(E/\tau)^{0.32},\ r = 0.94.$$

The higher exponent value and the better correlation both suggest that yield strength exerts a significant influence on the cratering process.

Figure 7 shows central mound height scaled against energy and viscosity. The correlation of r = 0.95 is better than that for the gravity scaling in Fig. 5, although

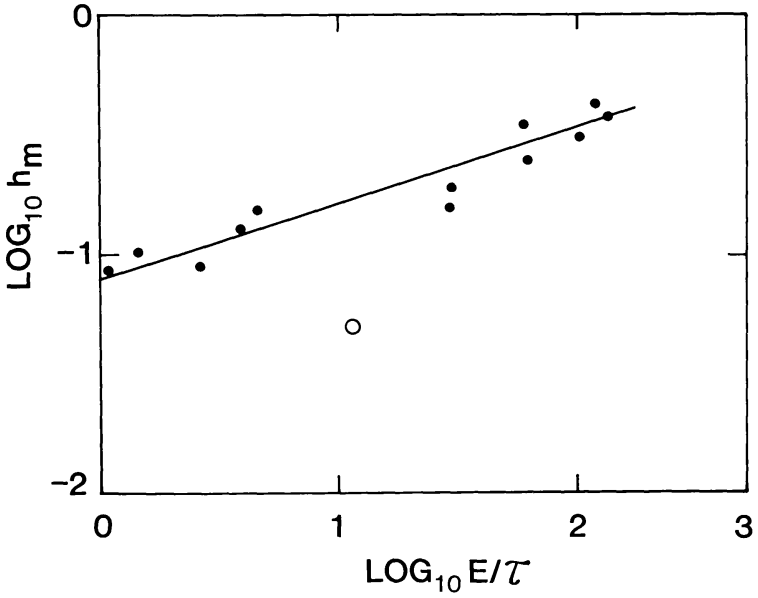

Fig. 6. Plot of maximum central mound height (h_m) as a function of target yield strength (τ) and energy (E); correlation coefficient = 0.94.

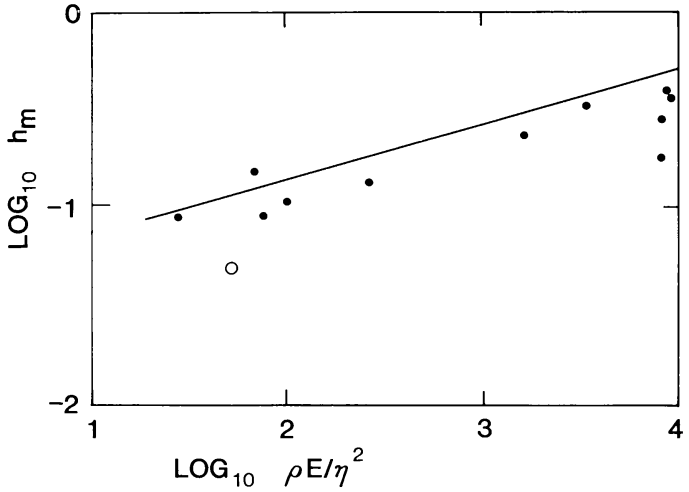

Fig. 7. Plot of maximum central mound height (h_m) as a function of target density (ρ), energy (E) and apparent viscosity (η); correlation coefficient = 0.95.

the power law exponents, n, are closer to the 0.25 characteristic of gravity scaling than to the 1.0 for viscous scaling:

$$h_m = (.04)\left(\frac{\rho E}{\eta^2}\right)^{0.28}, \; r = 0.95.$$

Thus it appears that in these experiments the target behaved more as an inviscid fluid than as a viscous one. In those runs where viscous forces dominated, the mound height was greatly reduced or nonexistent. We infer that in order to form "ejecta flow" craters through the agent of an oscillating central mound (see next section) gravitational effects must greatly outweight viscous ones. Choosing a typical martian multilobed crater, ~18 km diameter Yuty crater, we can roughly compute gravitational and viscous stresses as follows. Based on our experiments (Table 1) central mound height is approximately equal to ⅓ the crater diameter so that Yuty might have had a 6 km high transient central mound. Assuming the bulk density of martian surface material to be at least 1500 kg-m^{-3} (measured value for martian soil, Moore *et al.*, 1977) and g = 3.8 m-s^{-2}, we calculate the conditions under which $\rho gh \gg \eta^2/\rho h_m^2$. Substitution yields a maximum apparent viscosity of 10^9 kg-m^{-1}-s^{-1} or 10^{10} poises. Johnson (1970, p. 513) calculated a plastic viscosity (see Appendix) of about 10^3 poises and an apparent viscosity of about 10^4 poises for a debris flow in California. Thus if the rheological behavior of the impacted martian crust were comparable to that of terrestrial debris flows, we could expect gravitational effects to predominate over viscous ones.

4.0 DISCUSSION AND PLANETARY IMPLICATIONS

The general objective of the experiments was to determine the morphology of impact craters formed in viscous targets. The results described above apply to

the laboratory models. Extrapolation to planetary scales requires a host of dimensionless parameters, few of which can be satisfied simultaneously. Nonetheless, the experiments provide qualitative insight into the general processes involved and, through the isolation and study of individual parameters, some understanding can be gained of the processes involved in the formation of martian multilobed craters and of the effects of target viscosity on morphology (Boyce and Roddy, 1978). Photogeologic studies show that there is more than one type of martian multilobed crater (Carr *et al.*, 1977; Mouginis-Mark, 1979, Mouginis-Mark and Head, 1979; and others) and therefore it may not be appropriate to attempt to derive a single model of formation. Rather, once the morphologic types are fully classified, individual models may be required to explain each class. Until such a classification is developed, we prefer to discuss elements of multilobed craters and to suggest the implications of our experiments for those elements.

The primary characteristic of multilobed craters is the flow-like ejecta. Martian ejecta deposits consist of several facies, not all of which are necessarily present around all craters: 1) bright ray patterns; 2) deposits from secondary cratering; 3) isolated, detached flow lobes; and 4) flow lobes of continuous ejecta (which can occur in multiple tiers). Radial striations can occur on some or all of the flow lobes.

Bright ray patterns (Fig. 8) are similar to those observed around lunar and mercurian craters. Although rare on Mars, where rays do occur, they commonly are overlain by ejecta flow lobes or other ejecta deposits. Rays may be present on craters of equal size and located on apparently similar geologic material in the same area, suggesting that changes in target properties influence their development. We suggest that the bright rays are formed by ejection of an upper "dry" regolith or surface layer during the initial high velocity phase of ejecta excavation, comparable to impact cratering on the moon, and consist of both ejecta and mixing of local materials. The initial ejecta would be thrown farthest (ejected at highest velocities), followed by excavation of deeper, viscous material to form the flow-type deposits. Thus, the presence and degree of development of bright rays could be a function not only of stage of preservation (age), but the presence and thickness of a "dry" upper layer.

Detached ejecta deposits isolated from the main part of the ejecta field occur around many martian multilobed craters. These patches appear to be *primary* features rather than remnants of an eroded continuous ejecta blanket (Arvidson *et al.*, 1976). In the experiments the ejecta plume for fluid targets tears into descrete clots (Gault and Greeley, 1978), which impact the surface as separate units (Fig. 2). At the scale of martian craters, such clots may not remain as a single coherent large mass but disperse into a system of smaller clots (Schultz and Gault, 1979). Nevertheless, dependent on the degree of dispersion, upon impact they could coalesce and produce the detached ejecta clumps observed around certain martian craters.

The main ejecta deposit (Fig. 1) can be derived from two sources: 1) the initial ejecta plume, and 2) post-ejecta plume deposits. The initial ejecta plume deposits are emplaced ballistically on the surface. Once on the surface, however, they

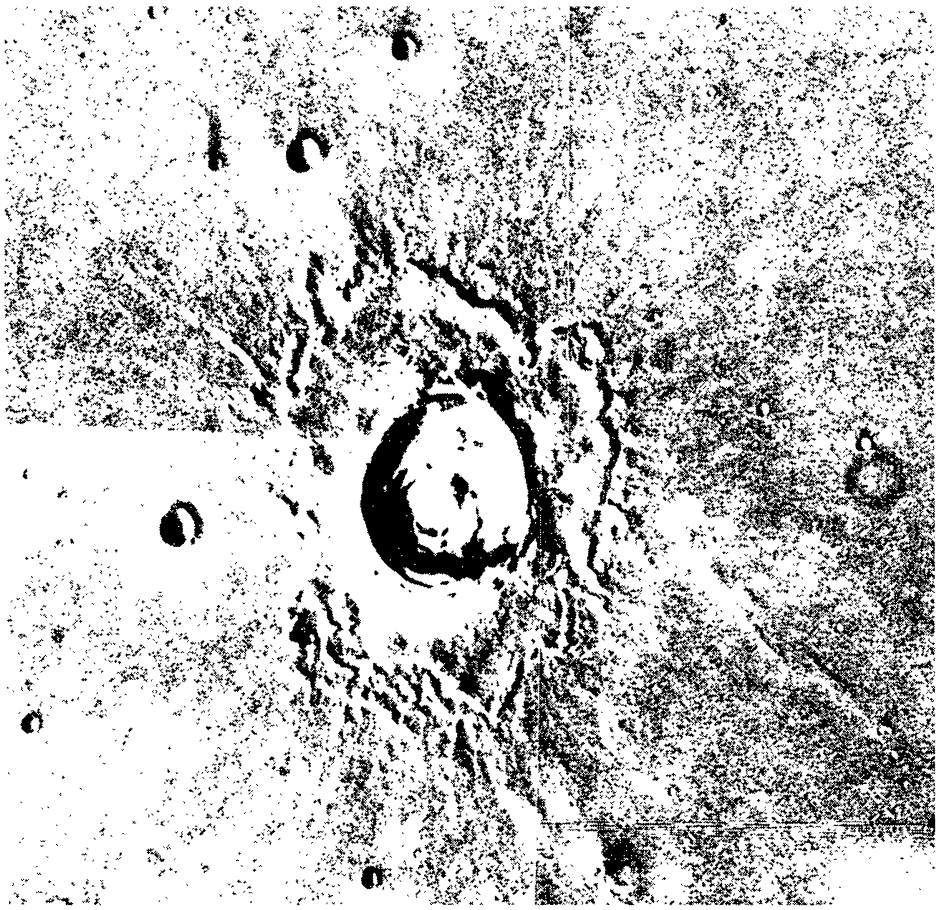

Fig. 8. Martian multilobed crater (~8 km in diameter) showing bright ray pattern interpreted to result from initial ejecta being derived from an upper "dry" regolith layer; deeper excavation penetrates volatile rich material that is emplaced as a fluidized mass which overrides part of the bright ray material. (VO 10A 21,22,23).

may behave similarly to landslides assuming the following conditions: 1) the ejecta mass consists of fragmental debris, possibly containing entrained volatiles [gases, water, melt-water (Carr *et al.*, 1977)], 2) the region around the crater is still seismically active (Schultz and Gault, 1975) from the impact as the ejecta plume material is being deposited, and 3) the mass is oversteepened on the rim of the crater; all three conditions favor mass wasting processes (Sharpe, 1938). In addition, possible early arrival of certain ejecta fractions in layered lithologies may form a lubricating layer of material (Schultz and Gault, 1979) that would enhance mass wasting. The third factor, oversteepening, results from: 1) the higher gravity on Mars causing deposition closer to the crater rim than in the lunar case, 2) the presence of an atmosphere which may cause deceleration of the finer size ejecta, including dispersed water droplets and vapor (Schultz and Gault, 1979) and its subsequent deposition closer to the crater, and 3) as suggested by the experiments, the ejecta plume angle varies inversely with the viscosity; thus the ballistic trajectory of low viscosity plume material would be at a high angle with deposition near the rim. Given these conditions, we assume that ejecta plume deposits can

be treated essentially as landslides, thus accounting for the flow-like characteristics previously described (Carr *et al.*, 1977). Although we envision these deposits to be emplaced early in the sequence, the unstable deposits could fail and flow conceivably any time in the history of the crater, and more than one failure could occur in the same mass to produce overlapping flow lobes.

The second source for the main mass of ejecta could be the collapsing central mound; the size of the rebounding central mound and the extent of the surge deposit resulting from its collapse vary inversely with the viscosity of the target. Although this deposit would be superposed on the ejecta plume deposit, its lateral extent would be less. It is conceivable, however, that the surge deposit could extend beyond the continuous plume deposits if it were derived from a deep, highly fluidized substratum. Although some estimates of ejecta blanket areas versus crater areas and volumes (Mutch and Woronow, 1980; Mouginis-Mark and Carey, 1980) have been made, a rigorous analysis of the volumes has not been performed. However, first order estimates (Fig. 9) of ejecta volume for several martian multilobed craters exceed by several times the volume of the crater bowl (even taking into account the transient crater volume and "bulking" of the ejecta), suggesting that flow of subsurface material during the excavation stage has occurred.

An oscillating central mound, similar to that observed in the experiments, could

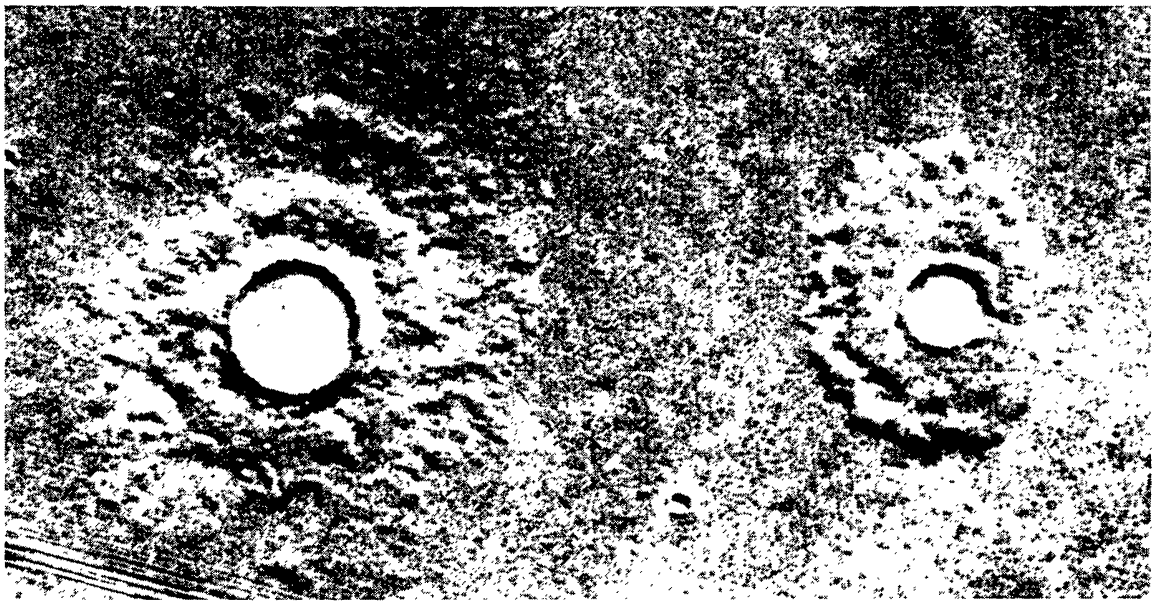

Fig. 9. Two martian craters for which estimated ejecta volumes exceed maximum calculated volume of crater bowl, even taking into account "bulking" of ejecta and uncertainties inherent in determining vertical lengths from shadow measurements. Crater at left is 4.8 km in diameter by 0.2 km deep, giving a maximum crater volume (assuming a hemispherical bowl shape) of 28.9 km^3, ejecta volume is estimated to be 38.8 km^3; 3.8 km diameter crater at right has a minimum volume of 1.4 km^3, a maximum volume of 7.1 km^3, and an ejecta volume of 38 km^3. Thus, some mechanism is required other than "normal" excavation to account for excess volume. We interpret excess to result from subsurface flow of material during uplift of the central mound.

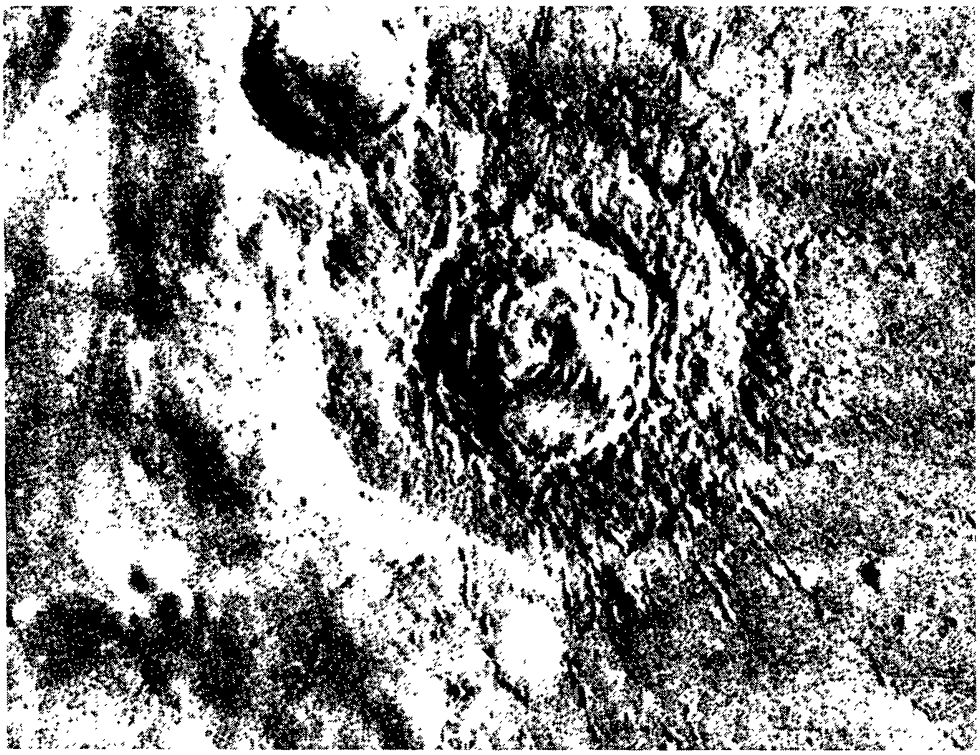

Fig. 10. A 35 km-diameter crater southeast of Amazonis Planitia showing well-developed interior terraces and slumping of the wall in large competent blocks, and lunar-type secondary craters; martian craters of this type appear to lack well developed multiple flow lobes (although an outer scarp of ejecta is present), and may reflect impact into materials having less volatiles than those in which multilobed craters form. (VO Frame 635A82).

account for the formation of the multiple tiers of ejecta lobes. We point out that in the experiments vigorous oscillations involved very fluid targets in which the crater rim was rarely preserved. Although some of the oscillations in the experiments were probably due to waves reflected from the walls and floor of the target bucket, in some respects this could be analogous to reflected energy from a competent rock stratum underlying unconsolidated volatile-rich material. We note that a model involving an oscillating central peak has been proposed to explain certain multi-ringed basins (Murray, 1980).

The emplacement mechanisms for the main ejecta mass described here involve flow of debris comparable to mass wasting. Striations observed on some ejecta lobes of martian craters may be shear lines similar to those that occur in landslide masses. However, striations on certain ejecta lobes appear to cross continuously both the inner lobes and outer lobes. This continuity may reflect shear lines propagated upward through overlying lobes, or as suggested by Mouginis-Mark (1980) and Singer and Schultz (1980), they may reflect scour marks by late-stage ejecta emplacement.

Although a planet-wide analysis has not been carried out, some martian craters show extensive wall slumping and interior terraces, tend to have less well developed multiple ejecta flow lobes, and tend to display secondary crater fields more typical of lunar and mercurian impact craters (Fig. 10). We interpret these

craters to have formed in more competent materials than that of the typical multilobed crater. Where such craters exist near multilobed craters on the same geological unit, it suggests that the target properties may have changed with time such as loss or gain of subsurface volatiles, with or without a change in atmospheric density. Conversely, the walls of many multilobed craters lack multiple terraces and have shallow, flat floors that appear to be flooded, perhaps as a result of local target degassing from the impact and its fluidization, comparable to that observed in the experiments.

5.0 CONCLUSIONS

The impact experiments in viscous targets produced results that at least qualitatively suggest mechanisms of formation for some of the martian multilobed craters and their associated features. Furthermore, some of the results may have a bearing on problems of large impact craters (i.e., basins) and the formation of multiple rings and impacts into "magma oceans" or accumulations of semimolten lava. The experiments almost certainly have implications for impacts into icy and ice-silicate bodies such as Ganymede and Callisto. The difficulty in applying the experimental results lies in scaling time, size and material properties to planetary conditions. Such problems, however, occur in all modeling, and can be overcome partly through dimensional analysis. We are continuing these analyses, and concurrently conducting impacts into targets including layers of differing viscosities to simulate multilayered ice/silicate mixtures, and other more complex planetary crusts.

Acknowledgments—Many people contributed to the successful completion of the experiments described here. We thank first the staff of the NASA-Ames Vertical Ballistic Gun Facility for their ready willingness to accomodate our needs; C. Wilbur and P. Spudis aided in the fabrication of special target buckets; R. Leach and M. Plummer assisted with the measurements of the rheological properties of the various mixtures; T. Timmcke assisted in some of the measurements taken from the motion pictures; V. Sisson, Planetary Geology Summer Intern, assisted with the first series of experiments. Finally, we thank all who got their hands in the mud and who helped clean up after the experiments. This work was supported by NASA grants NSG-7429, NSG-7415, and NAGW-56.

The Lunar and Planetary Institute is operated by the Universities Space Research Association under Contract No. NSR 09-051-001 with the National Aeronautics and Space Administration. This paper constitutes the Lunar and Planetary Institute Contribution No. 417.

REFERENCES

Arvidson R. E., Coradini M., Carusi A., Caradini A., Fulchignoni M., Federico C., Funiciello R., and Salomone M. (1976) Latitudinal variation of wind erosion of crater ejecta deposits on Mars. *Icarus* **27**, 503–516.

Boyce J. M. and Roddy D. J. (1978) Martian rampart craters: crater processes that may affect diameter-frequency distributions (abstract). Reports of Planetary Geology Program 1977-1978, p. 162–165. NASA TM-79729.

Carr M. H., Crumpler L. S., Cutts J. A., Greeley R., Guest J. E., and Masurky H. (1977) Martian impact craters and emplacement of ejecta by surface flow. *J. Geophys. Res.* **82,** 4055–4065.

Gault D. E. (1973) Displaced mass, depth, diameter, and effects of oblique trajectories for impact craters formed in dense crystalline rocks. *The Moon* **6,** 32–44.

Gault D. E. and Greeley R. (1978) Exploratory experiments of impact craters formed in viscous-liquid targets: Analogs for martian rampart craters. *Icarus* **34,** 486–495.

Gault D. W., Quaide W. L., and Oberbeck V. R. (1968) Impact cratering mechanics and structures. In *Shock Metamorphism of Natural Materials* (B. M. French and N. M. Short, eds.), p. 87–99. Mono, Baltimore.

Gault D. E. and Wedekind J. A. (1977) Experimental hypervelocity impact into quartz sand, II: Effects of gravitational acceleration. In *Impact and Explosion Cratering* (R. O. Pepin and R. B. Merril, eds.), p. 1231–1244. Pergamon, N.Y.

Gault D. E., and Wedekind J. A. (1978) Experimental impact "craters" formed in water: Gravity scaling realized. *EOS (Trans. Amer. Geophys. Union)* **59,** 1121.

Grimshaw R. W. (1971) *The Chemistry and Physics of Clays.* Wiley, N.Y. 1024 pp.

Hulme G. (1974) Interpretation of lava flow morphology. *Geophys. J. Roy. Astron. Soc.* **39,** 361–383.

Johansen L. A. (1978) Martian splosh cratering and its relation to water. *Proc. Second Colloqium on Planetary Water and Polar Processes,* p. 109–110. Hanover, N.Y.

Johnson A. M. (1970) *Physical Processes in Geology.* Freeman, San Francisco. 577 pp.

Moore F. (1965) *Rheology of Ceramic Systems.* MacLaren, London. 78 pp.

Moore H. J., Hutton R. E., Scott R. F., Spitzer C. R., and Shorthill R. W. (1977) Surface materials of the Viking Landing Sites. *J. Geophys. Res.* **82,** 4497–4523.

Mouginis-Mark P. (1979) Martian fluidized crater morphology: variations with crater size, latitude, altitude and target material. *J. Geophys. Res.* **84,** 8011–8022.

Mouginis-Mark P. (1980) An emplacement sequence for martian fluidized ejecta craters (abstract). In *Lunar and Planetary Science XI,* 753–755. Lunar and Planetary Institute, Houston.

Mouginis-Mark P. J. and Carey D. L. (1980) Volume estimates of fluidized ejecta deposits in the northern plains of Mars (abstract). In *Lunar and Planetary Science XI,* 759–761. Lunar and Planetary Institute, Houston.

Mouginis-Mark P. J. and Head J. W. (1979) Emplacement of martian rampart crater ejecta blankets: A morphological analysis (abstract). In *Lunar and Planetary Science X,* 870–872. Lunar and Planetary Institute, Houston.

Murray J. B. (1980) Oscillating peak model of basin and crater formation. *Moon and Planets* **22,** 269–291.

Mutch P., and Woronow A. (1980) Martian rampart and pedestal craters ejecta-emplacement: Coprates Quadrangle. *Icarus* **41,** 259–268.

van Olphen H. (1977) *An Introduction to Clay Colloid Chemistry.* Wiley, N.Y. 318 pp.

Roddy D. J., Arthur D. W. G., Boyce J. M., Pike R. J., and Soderblom L. A. (1979) Martian impact cratering: Preliminary report (abstract). Reports of Planetary Geology Program 1978–1979, p. 187–189. NASA TM-80339.

Schultz P. H. and Gault D. E. (1975) Seismic effects from major basin formations on the Moon and Mercury. *The Moon* **12,** 159–177.

Schultz P. H. and Gault D. E. (1979) Atmospheric effects on martian ejecta emplacement. *J. Geophys. Res.* **84,** 7669–7687.

Scott R. (1967) Viscous flow of craters. *Icarus* **7,** 139–148.

Sharpe C. F. S. (1938) *Landslides and Related Phenomena.* Columbia Univ. Press. N.Y. 137 pp.

Shaw H. R., Wright T., Peck D., and Okamura R. (1968) The viscosity of basaltic magma: An analysis of field measurements in Makaopuhi Lava Lake, Hawaii. *Amer. J. Sci.* **266,** 225–264.

Singer J. and Schultz P. H. (1980) Secondary impact craters around lunar, mercurian and martian craters (abstract). In *Lunar and Planetary Science XI,* 1042–1043. Lunar and Planetary Institute, Houston.

van Wazer J. R., Lyons J. W., Kim K. Y., and Caldwell R. E. (1963) *Viscosity and Flow Measurements.* Wiley, N.Y. 406 pp.

Appendix
RHEOLOGY OF EXPERIMENTAL TARGET MATERIALS

An underlying assumption of our experiments was that the formation of multilobe craters requires a target which can behave both as a fluid to produce the observed flow patterns around obstacles and as a solid to produce the steep flow lobe fronts. Without specifying the composition of such a material, we can characterize its rheology by the Bingham model. A Bingham material deforms either as an elastic solid or a linearly viscous fluid, depending upon whether the applied shear stress is greater or less than a critical value called the yield strength, τ_y. For stress greater than τ_y, strain rate is proportional to applied stress and the proportionality constant is the plastic viscosity, η_p; below τ_y, no permanent deformation occurs. Bingham materials are thus characterized by these two material constants, τ_y and η_p. This plastic viscosity has the same dimensions as Newtonian viscosity and is a measure of a Bingham body's resistance to flow. Clay suspensions were selected as target materials because they commonly exhibit Bingham behavior.

Four groups of clay suspensions were made by combining one of two commercially available clay bodies with either water or silicon oil. The suspensions were mixed at the test facility using a power drill with a stirring attachment. The consistencies of the slurries were varied by adding more dry clay or more fluid (oil or water) to the containers and restirring.

In general, clay slurries exhibit a continuous range of flow properties from viscous to plastic, depending primarily on the concentration of suspended particles and their degree of interaction (Grimshaw, 1971). At volume concentrations of less than about 2 percent solids, clay slurries have a Newtonian viscosity which varies linearly with the concentration (Moore, 1965). At increasing clay concentrations the particles begin to inferfere with one another, leading to an exponential variation of viscosity with concentration. At about 30 percent solids many clay suspensions begin to develop an internal structure and an associated yield strength. This yield value increases roughly as the third power of the concentration (Moore, 1965). At high concentrations some clay suspensions may show strongly nonlinear behavior, in which the strain rate is proportional to the applied stress raised to some power ($\epsilon = |\sigma|^n$; ϵ = strain rate; σ = stress), the sign of n depending on the mineralogy of the clay particles. Time dependent effects are sometimes observed, caused by changes in yield strength accompanying increased duration of shearing stress.

These relationships between rheologic properties and other factors were determined under ideal laboratory conditions. Measurements made during our experiments were much less well controlled and several of the required experimental procedures could lead to inadvertant rheologic changes. It is impossible to monitor continuously all of the effects, and rheologic measurements must be taken for every batch of slurry used in the runs. Here we list some of the changes in viscosity and yield strength that might be expected in the preparation of our target materials.

During our experiments we frequently altered the concentration of the slurries, thus changing the rheologic properties. After energetic shots, much clay was expelled from the target bucket and had to be replaced. Homogenization of the slurry was then accomplished by stirring at very high speeds which could cause both the viscosity and yield strength to decrease in proportion to the amount of time of stirring, perhaps because interparticle forces are reduced. As the mixed clay is allowed to rest, its strength and viscosity may rise by an amount dependent upon the time of standing. In addition, large amounts of air are inadvertantly mixed into the slurry during stirring which also decreases both rheologic parameters. This effect is partly reversed by exsolution of the gas during periods when the clay is not being worked. Depressurization of the chamber before impact also promotes degassing which often leads to stiffening of the clay. In those experiments where a stiff surface layer of sand or clay was added, mixing in some of the stiffer component inevitably occurred after impact, raising the bulk viscosity of the slurry. Similarly, targets with icy surface layers also led to a higher viscosity and strength after impact.

Very high shear stresses are generated locally at the site of impact, where nonlinear effects might cause the actual viscosity to be different from that recorded either immediately before or after the shot. However, our rheologic measurements indicated that these power law effects were minimal in the slurries we used. The temperature of the slurries ranged over about 8°C during the course of the experiments. Within this range, the viscosities would not be greatly influenced (van Olphen, 1977).

Rheologic measurements

Rheologic data were collected using a Brookfield Model HBT Synchrolectric Viscometer with a Helipath attachment which allows measurement in highly viscous fluids. The viscometer rotates a spindle in the fluid and measures the torque necessary to overcome the viscous resistence to the induced movement. The spindles consist of a cylinder with either a disk or t-bar at the base. Neither of these geometries allows simple computations of the viscosity (van Wazer *et al.*, 1963). The torque readings indicate the "instrument viscosity" (Shaw *et al.*, 1968) which can be converted to the absolute viscosity for Newtonian fluids and the apparent viscosity for non-Newtonian fluids. The apparent viscosity is the ratio of total shear stress to shear rate and is not a material constant for non-Newtonian fluids. At a stated shear rate, however, it provides a measure of the fluid's resistance to flow that allows intercomparisons with other similar fluids. For Bingham materials, plastic viscosity and yield strength must be determined by indirect methods.

We attempted to calculate the Bingham properties of the clay slurries by following a procedure described by Hulme (1974). First the instrument readings were converted to absolute force values through calibration with a known mass and the force of gravity. Then, for the disk-type spindles, the area was measured and stress was computed by dividing the force by this area. Strain rate was equated with the measured rate of rotation of the shaft, and a plot of shear strain rate versus stress was constructed. These plots conformed to those expected for a Bingham material, and values of yield strength and plastic viscosity could be measured directly from the plots.

Although this procedure indicated Bingham-like properties, it has three inherent problems. First, the computations were only made for batch samples collected every 2 to 8 shots during the first series of experiments (runs 1–55) and thus represent average values which might not adequately reflect rheologic conditions specific to each run. Second, surface areas could only be measured for the disk-type spindles which could not be used for the more viscous target materials. Third, the actual strain rate varies widely across the radius of the cup holding the test fluid, and the calculated values were valid only at the shaft. Despite these limitations, we were able to characterize the relative rheologic properties of the target materials for the first series of experiments.

In subsequent experiments, including those currently underway, we are attempting to eliminate some of these difficulties. As an alternative to the calculated plastic viscosity values, we are using instrument viscosity data collected for every target material. Relative yield strengths are being measured directly by using the cone indentation method (Moore, 1965). We do not yet have a means of computing the effective areas of the t-bar spindles, but if the same spindle is used for all measurements, then the *relative* viscosities should produce internally consistent results. Presumably, the functional relationships indicated by these data will also apply to absolute measurements, differing by some as yet unknown constant. At this stage we are investigating these functional relationships. In our ongoing experiments we are attempting to determine the absolute values of the variables so that we can better scale our results to martian conditions.

Experimental data

Table 1 lists the experimental data. Impact conditions and target properties were set prior to each shot; crater morphology was measured after impact, and the geometry of the transient structures such as central peaks and surge waves was observed in high speed motion pictures. Each successful run (no misfires) was assigned a number. Runs 1–55 (series 1) were carried out in June and July, 1979. Rounds 56–75 (series 2) were conducted in December 1979. In the first set of experiments, plastic viscosities and yield strengths were calculated for average batches of target materials, as described earlier. Apparent viscosities at a single RPM value were measured for each target. During the second set, complete determinations were made for each shot. In multilayer configurations the properties of both slurries were determined.